Investigation on Characteristics and Optimal Shapes of Interior PM Synchronous Motor for Electric Vehicle Application

S. I. Kim[1], *Student Member, IEEE*, J. P. Hong[1], *Senior Member, IEEE*, and J. Hur[2], *Senior Member, IEEE*
[1]Department of Automotive Engineering, Hanyang University, Seoul, 133-791, Korea
ksi1976@dreamwiz.com, hongjp@hanyang.ac.kr
[2]Artificial Intelligent & Mechatronics Research Center, Korea Electronics Technology Institute, Puchon, 420-140, Korea

***Abstract*-The torque ripple of interior PM synchronous motor (IPMSM) operated in wide speed range through flux weakening variously varies according to operating point. That is mainly generated because of the difference of magnetic saturation in each point. Moreover, from the torque performance point of view, the IPMSM with concentrated winding is relatively disadvantage compared with that with distributed winding and surface PM synchronous motor. Therefore, in this paper, each optimal model minimizing torque ripple at the base and maximum speed and cogging torque is investigated by an optimization method. In addition, the characteristics of each model are compared by finite element analysis and characteristic equation. In the end, the final results show the optimal shape according to the operating point of IPMSM must be changed to satisfy torque performance.**

I. Introduction

The main capabilities required in the applications such as traction motor for a hybrid electric vehicle and ISG (integrated starter generator) are wide constant power speed range (CPSR) and high efficiency. Interior PM synchronous motor (IPMSM) is one of the motors suitable for the applications [1]. From the torque performance point of view, however, the IPMSM has two drawbacks. That is, torque ripple and cogging torque are relatively large as compared with a surface PM synchronous motor. Moreover, the IPMSM with concentrated winding is more disadvantageous than that with distributed winding in the respects [2]. These problems are produced mostly by the discontinuous reluctance variation because of the slotted structure of stator core and saturation of magnetic circuit [2], [3]. Particularly, the magnetic saturation of the IPMSM operated in wide speed range through flux weakening control greatly varies according to load condition. Thus, the optimal design of IPMSM is demanded in order to improve torque performance.

In this paper, each optimal model minimizing torque ripple at the base and maximum speed and cogging torque is investigated by an optimization method without a great change of the motor parameters in the initial designed IPMSM. In addition, the characteristics of each model are compared by finite element analysis (FEA) and characteristic equation. In the end, the final results show the optimal shape according to the operating point of IPMSM must be changed to enhance torque characteristic.

II. Initial Model and Equivalent Circuit

Fig. 1 displays the configuration of the initial designed IPMSM with concentrated winding. The CPSR of the initial model is from 680 rpm to 3400 rpm, and the main dimension and specifications are listed in Table I.

Equivalent circuits for the characteristic analysis of the IPMSM are shown in Fig. 2 [4]. The equivalent circuits include the effects of the copper loss and the iron loss. From Fig. 2, the voltage and effective torque equation of the IPMSM in the steady-state are expressed as follows:

$$\begin{bmatrix} v_d \\ v_q \end{bmatrix} = R_a \begin{bmatrix} i_{od} \\ i_{oq} \end{bmatrix} + \left(1 + \frac{R_a}{R_c}\right) \begin{bmatrix} v_{od} \\ v_{oq} \end{bmatrix} \tag{1}$$

$$\begin{bmatrix} v_{od} \\ v_{oq} \end{bmatrix} = \begin{bmatrix} 0 & -\omega L_q \\ \omega L_d & 0 \end{bmatrix} \begin{bmatrix} i_{od} \\ i_{oq} \end{bmatrix} + \begin{bmatrix} 0 \\ \omega \psi_a \end{bmatrix} \tag{2}$$

$$T = P_n[\psi_a i_{oq} + (L_d - L_q) i_{od} i_{oq}] \tag{3}$$

where i_d, i_q: d- and q-axis components of armature current; i_{cd}, i_{cq}: d- and q-axis components of iron loss current; v_d, v_q: d, q components of terminal voltage; ψ_a: $\sqrt{3/2}\,\psi_f$; ψ_f: maximum flux linkage of permanent magnet; R_a: armature winding resistance; R_c: iron loss resistance; L_d, L_q: inductance along d-, q-axis; P_n: number of pole pairs.

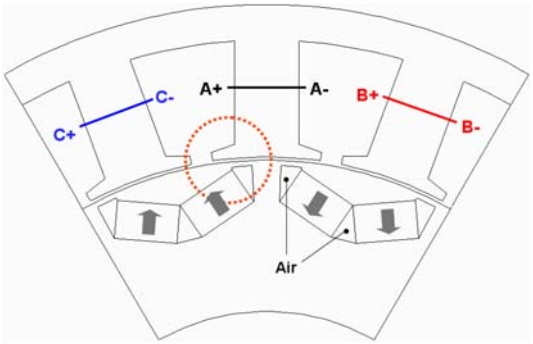

Fig. 1. Configuration of initial designed IPMSM.

TABLE I
SPECIFICATIONS OF INITIAL DESIGNED IPMSM

Items	Values
Stator outer diameter	292 mm
Rotor outer diameter	204.8 mm
Stack length	85 mm
Air-gap	0.9 mm
Br (@120°C)	1.103 T
Number of poles	12
DC link voltage	320 V
Rated output power	20 kW
Rated current	70 A_{rms}
Base and maximum speed	680, 3400 rpm

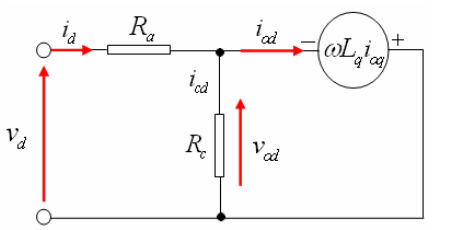

(a) d-axis

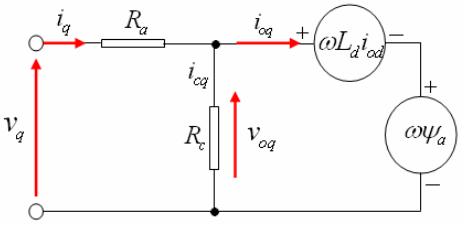

(b) q-axis

Fig. 2. Equivalent circuits of IPMSM.

III. PARAMETER CALCULATION METHOD AND INITIAL CONDITIONS FOR OPTIMIZATION

There are four parameters, ψ_a, R_a, R_c, L_d and L_q, needed to solve the circuit models of Fig. 2. In this paper, the estimation method on two parameters of them, iron loss resistance and inductances, is introduced, and then the characteristics of the initial model obtained by the circuits based on the parameters are finally displayed in Section V.

A. Equivalent Iron Loss Resistance, R_c

Fig. 3 shows the procedure of iron loss calculation using iron loss data of magnetic material. The detail explanation as regards the flowchart has been given in [5]. After calculating total iron loss, w_{total}, the iron loss resistance R_c is calculated by (4).

$$R_c = v_0^2 / w_{total} \tag{4}$$

where v_0 is terminal voltage at the no load and 1000 rpm.

B. Inductances, Ld and L_q

At the base and maximum speed, input armature current and current angle (β) are demanded to estimate accurately torque ripple by FEA. To get them, L_d and L_q must be computed according to the variation of armature current and β. In this paper, they are obtained by FEA, cubic spline interpolation and (5). In (5), ψ_a and ψ_o are fundamental components calculated from fourier analysis. The steady-state phasor diagram of IPMSM is shown in Fig. 4 [6].

$$L_d = \frac{\psi_o \cos\alpha - \psi_a}{i_d} \qquad L_q = \frac{\psi_o \sin\alpha}{i_q} \tag{5}$$

where ψ_o: total flux linkage considering the armature reaction effects; α: phase difference between ψ_a and ψ_o.

C. Results of Initial Model by Characteristic Equation

The characteristics of the initial model are predicted with L_d and L_q estimated through the way mentioned above. At this time, the limitations on armature current and terminal voltage are considered as (6) and (7), and in this stage, all the losses except the copper loss are ignored.

$$I_a = \sqrt{i_d^2 + i_q^2} \le I_{am} \tag{6}$$

$$V_a = \sqrt{v_d^2 + v_q^2} \le V_{am} \tag{7}$$

where I_{am}, V_{am}: peak values of current and voltage.

The entire torque-speed operation region considering the above control conditions is acquired as the following manner. In the anterior region of base speed, maximum torque per ampere control is used, and flux weakening control is applied in the posterior region. In the end, the characteristics obtained from the initial model satisfy the specifications given in Table I, and torque ripple at the base and maximum speed and peak value of cogging torque are 22 %, 184 % and 4.03 Nm respectively. At that time, input current is 64.2 A and 63.1 A, and β is 39.2° and 80.6°, and the optimization process of the IPMSM is based on these results.

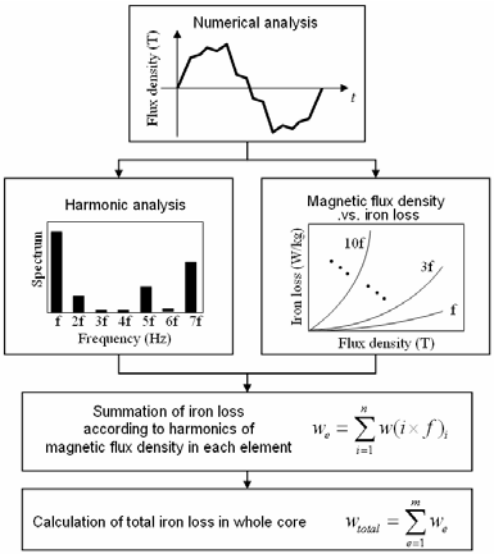

Fig. 3. Calculation process of iron loss.

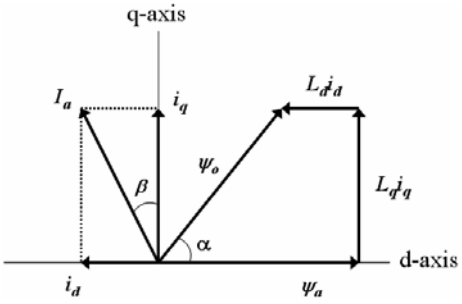

Fig. 4. Phasor diagram of IPMSM.

IV. Optimization

A. Design Variables for Optimization

In the IPMSM, the operating limits, restrictions on current and terminal voltage, and CPSR critically depend on the motor parameters such as flux linkage generated by permanent magnet and inductance [7]. Therefore, in the initial model, the size and position of permanent magnet and air-gap length are not changed, because they greatly affect the parameters. Due to fill factor, the teeth and yoke width are not altered as well. Thus, design variables selected in this paper are barrier angle (BA), chamfer (C), slot opening (SO). Fig. 5, the magnified figure of the part surrounded a dotted line in Fig. 1, shows them.

B. Experimental Design

In this paper, full factorial design (FFD), one of the experimental designs, is used, and the reason is written as follows. First, all combinations of the design variables chosen in the initial model are inspected, and interaction effects between them are evaluated without confounding. Moreover, the main factors on torque ripple and cogging torque are detected by analysis-of-variance (ANOVA). Second, the prediction of the responses according to the variation of the design factors is possible. Finally, the effective and reasonable design area is selected to apply response surface method (RSM) [8], [9]. In the motor design, to research the full design region needs a lot of modeling and computing time. In addition, in RSM, the accuracy of approximation greatly depends on the size of the space in which the design parameters may vary [10]. Accordingly, FFD is performed in the wide domain, and then RSM is applied in the best region searched by that. Table II shows the array of 2^3 FFD to examine torque ripple and cogging torque. In the table, experiment No. 9 is added to estimate the curvature in the middle point of each design area, because it is performed at only two levels. In this paper, the levels are called "low" and "high" and denoted as "–1" and "+1" respectively.

In this paper, ANOVA is applied to evaluate more objectively the significance of each design factor through statistical analysis. At that time, there is no replication of experiment. ANOVA table is shown in Table III. In the table, the sums of squares (*SS*) of each term and those of error and total term are given as follows:

$$SS_{term} = \frac{1}{N}\begin{bmatrix}(total\ sum\ of\ high\ levels)\\ -(total\ sum\ of\ low\ levels)\end{bmatrix}^2 \tag{8}$$

$$SS_E = SS_T - \begin{bmatrix}SS_{BA} + SS_C + SS_{SO} + SS_{BA*C}\\ + SS_{BA*SO} + SS_{C*SO}\end{bmatrix} \tag{9}$$

$$SS_T = \sum_{i=1}^{lmn} y_i^{\,2} - \frac{\left(\sum_{i=1}^{lmn} y_i\right)^2}{lmn} \tag{10}$$

where N: total number of trials; y_i: *i-th* response value in the experiment; l, m and n: the number of levels in factor BA, C and SO respectively.

The ANOVA results of each response are listed in Table IV, Table V and Table VI. Especially, in the tables, the important factors on the each response are indicated at 5% and 10% significance level [8].

Fig. 6 shows the variation of each response according to main factors based on ANOVA results. In Fig. 6. (c), the interaction effect plot between BA and C is displayed, and the peak-to-peak value of cogging torque is small overall when BA is 34.5°. However, in the value of BA, the aspects of torque ripple at the maximum speed and cogging torque according to C occur by contraries. Therefore, in the optimal stage applied with RSM, the scope of C is the same that used in FFD.

C. RSM

RSM is a set of statistical and mathematical techniques to find the "best fitted" response of the physical system through experiment or simulation. It has recently been recognized as an effective approach for modeling the performance of electrical devices.

In RSM, a polynomial model called a fitted model is generally to be constructed to represent the relationship between the performance and design parameters [9]. Thus, this model provides designers with an overall prospect of the performance according to the behavior of the factors in a design space. In this paper, RSM is employed to make appropriate response models with respect to torque ripple and cogging torque in the initial designed IPMSM. In general, the response model can be written as follows:

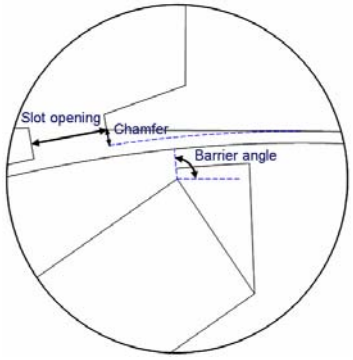

Fig. 5. Design variables for optimization.

TABLE II
ARRAY OF 2^3 FFD AND RESULTS

Experiment No.	BA[°] (level)	C[mm] (level)	SO[mm] (level)	BA*C (level)	BA*SO (level)	C*SO (level)	Torq. ripple[%] @ base speed	Torq. ripple[%] @ max. speed	Cogging $T_{p\text{-}p}$ [Nm]
1	34.5(-1)	0.5(-1)	4(-1)	(+1)	(+1)	(+1)	22.2	108.2	0.88
2	145.5(+1)	0.5(-1)	4(-1)	(-1)	(-1)	(+1)	22.8	109.4	8.76
3	34.5(-1)	1.5(+1)	4(-1)	(-1)	(+1)	(-1)	17.6	46.0	4.44
4	145.5(+1)	1.5(+1)	4(-1)	(+1)	(-1)	(-1)	17.2	49.0	4.63
5	34.5(-1)	0.5(-1)	8(+1)	(+1)	(-1)	(-1)	8.6	79.8	1.19
6	145.5(+1)	0.5(-1)	8(+1)	(-1)	(+1)	(-1)	10.3	91.3	6.86
7	34.5(-1)	1.5(+1)	8(+1)	(-1)	(-1)	(+1)	11.2	38.6	6.56
8	145.5(+1)	1.5(+1)	8(+1)	(+1)	(+1)	(+1)	10.6	45.9	5.90
9	90(0)	1.0(0)	6(0)	(0)	(0)	(0)	14.8	90.2	1.61

TABLE III
ANALYSIS OF VARIANCE

Terms	Sum of squares (*SS*)	Degree of freedom	Mean square	F_o
BA	SS_{BA}	$\phi_{BA} = l\text{-}1$	$MS_{BA} = SS_{BA} / \phi_{BA}$	MS_{BA} / MS_E
C	SS_C	$\phi_C = m\text{-}1$	$MS_C = SS_C / \phi_C$	MS_C / MS_E
SO	SS_{SO}	$\phi_{SO} = n\text{-}1$	$MS_{SO} = SS_{SO} / \phi_{SO}$	MS_{SO} / MS_E
BA*C	SS_{BA*C}	$\phi_{BA*C} = (l\text{-}1)(m\text{-}1)$	$MS_{BA*C} = SS_{BA*C} / \phi_{BA*C}$	MS_{BA*C} / MS_E
BA*SO	SS_{BA*SO}	$\phi_{BA*SO} = (l\text{-}1)(n\text{-}1)$	$MS_{BA*SO} = SS_{BA*SO} / \phi_{BA*SO}$	MS_{BA*SO} / MS_E
C*SO	SS_{C*SO}	$\phi_{C*SO} = (m\text{-}1)(n\text{-}1)$	$MS_{C*SO} = SS_{C*SO} / \phi_{C*SO}$	MS_{C*SO} / MS_E
Error	SS_E	$\phi_E = (l\text{-}1)(m\text{-}1)(n\text{-}1)$	$MS_E = SS_E / \phi_E$	
Total	SS_T	$\phi_T = lmn\text{-}1$		

TABLE IV
ANOVA RESULT ON TORQUE RIPPLE AT BASE SPEED

Terms	Sum of squares (*SS*)	Degree of freedom	Mean square	F_o	$F(\phi_{term}, \phi_E, 0.05)$	Significance?
BA	0.25	1	0.25	1.04	161	No
C	6.74	1	6.74	28.08	161	No
SO	190.24	1	190.24	792.67	161	Yes
BA*C	1.38	1	1.38	5.75	161	No
BA*SO	0.11	1	0.11	0.46	161	No
C*SO	21.72	1	21.72	90.5	161	No
Error	0.24	1	0.24			
Total	220.68	7				

TABLE V
ANOVA RESULT ON TORQUE RIPPLE AT MAXIMUM SPEED

Terms	Sum of squares (*SS*)	Degree of freedom	Mean square	F_o	$F(\phi_{term}, \phi_E, 0.05)$	Significance?
BA	66.3	1	66.3	15.35	161	No
C	5473.74	1	5473.74	1206.07	161	Yes
SO	406.31	1	406.31	94.05	161	No
BA*C	0.69	1	0.69	0.16	161	No
BA*SO	26.62	1	26.62	6.16	161	No
C*SO	161.55	1	161.55	37.4	161	No
Error	4.32	1	4.32			
Total	6139.53	7				

TABLE VI
ANOVA RESULT ON COGGING TORQUE

Terms	Sum of squares (*SS*)	Degree of freedom	Mean square	F_o	$F(\phi_{term}, \phi_E, 0.1)$	Significance?
BA	21.36	1	21.36	97.09	39.9	Yes
C	1.85	1	1.85	8.41	39.9	No
SO	0.4	1	0.4	1.82	39.9	No
BA*C	24.59	1	24.59	111.77	39.9	Yes
BA*SO	1.16	1	1.16	5.27	39.9	No
C*SO	3.09	1	3.09	14.05	39.9	No
Error	0.22	1	0.22			
Total	52.67	7				

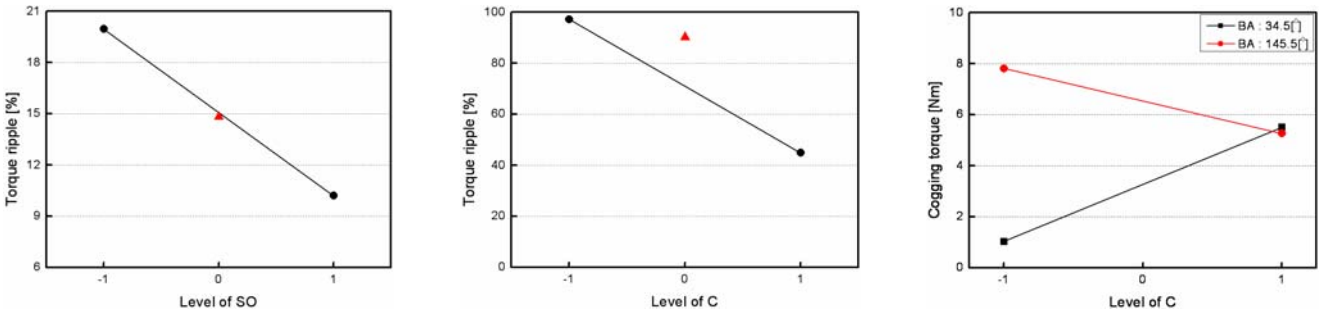

(a) Torque ripple @ base speed (b) Torque ripple @ maximum speed (c) Cogging torque

Fig. 6. Responses according to the variation of main factors.

$$Y = \beta_0 + \sum_{i=1}^{k} \beta_i x_i + \sum_{i=1}^{k} \beta_{ii} x^2{}_i + \sum_{i \neq j}^{k} \beta_{ij} x_i x_j + \varepsilon \quad (10)$$

where β is regression coefficients for design variables, ε is random error treated statistical error.

In this paper, least square method is utilized to estimate unknown coefficients, and the fitted coefficients and the fitted response model can be written as:

$$\hat{\boldsymbol{\beta}} = (\boldsymbol{X}'\mathbf{Y})^{-1} \boldsymbol{X}'\mathbf{Y} \quad (11)$$

$$\hat{\mathbf{Y}} = \boldsymbol{X}\hat{\boldsymbol{\beta}} \quad (12)$$

where $\boldsymbol{X}$: matrix notation of the levels of the independent variables; $\boldsymbol{X}'$: transpose of the matrix $\boldsymbol{X}$; $\mathbf{Y}$: vector of the observations.

Central composite design (CCD) is employed as the experimental design method to estimate the fitted model of each response [9]. CCD consists of three portions: a complete 2^k factorial design in which the factor levels are coded into –1 and 1; axial points at a distance α from the center point; one design center point. Table VII shows the design area of CCD based on FFD results. At that time, the width of SO is restricted to 9 mm to support coil in the slot.

From the above stated process, the polynomial models of the responses are given by (14), (15) and (16) respectively.

$$\hat{\mathbf{Y}}_{\text{Tr\_base}} = 48.4 + 0.16\text{BA} - 17.9\text{C} - 6.4\text{SO} - 0.002\text{BA}^2 + 4.1\text{C}^2 + 0.1\text{SO}^2 - 0.04\text{BA}\cdot\text{C} + 0.008\text{BA}\cdot\text{SO} + 1.7\text{C}\cdot\text{SO} \quad (14)$$

$$\hat{\mathbf{Y}}_{\text{Tr\_max}} = 145.8 + 2.1\text{BA} - 140.5\text{C} + 7.4\text{SO} - 0.03\text{BA}^2 + 5.7\text{C}^2 - 2.6\text{SO}^2 - 0.3\text{BA}\cdot\text{C} + 0.1\text{BA}\cdot\text{SO} + 12.2\text{C}\cdot\text{SO} \quad (15)$$

$$\hat{\mathbf{Y}}_{\text{CT}} = -11.7 + 0.3\text{BA} - 3.8\text{C} + 2.4\text{SO} - 0.003\text{BA}^2 + 2.5\text{C}^2 - 0.1\text{SO}^2 + 0.02\text{BA}\cdot\text{C} - 0.03\text{BA}\cdot\text{SO} + 0.3\text{C}\cdot\text{SO} \quad (16)$$

Table VIII displays the optimal points minimizing each response obtained by (14), (15) and (16), and Fig. 7 shows the results of each model corresponding to the point. As known in the results, the optimal conditions can not simultaneously minimize torque ripple at the base and maximum speed and cogging torque. Moreover, each optimal point with respect to torque ripple at the maximum speed and cogging torque is located contrastively. That means the appropriate trade-off is required according to the application of IPMSM. As SO is 8.68 mm, the variation of each response is shown in Fig. 8.

In each optimal point, the results from the polynomial models are compared with those of FEA in Table IX. From the comparison, the models are very useful to predict the responses in the region. That is also verified by the coefficient of determination called R^2 [9], [10]. It is the statistics index to evaluate the quality of the models. R^2 of each fitted model are 0.985, 0.996 and 0.927 respectively.

TABLE VII
DESIGN REGION OF CCD

Design factors	Levels of design factors				
	-α	-1	0	1	α
BA [°]	25.25	29	34.5	40	43.75
C [mm]	0.16	0.5	1.0	1.5	1.84
SO [mm]	5.32	6	7	8	8.68

TABLE VIII
OPTIMAL POINTS OF EACH RESPONSE

Design factors	Optimal point @ base speed	Optimal point @ max. speed	Optimal point @ cogging torque
BA [°]	25.25	25.25	43.75
C [mm]	0.53	1.84	0.5
SO [mm]	8.68	8.68	8.68

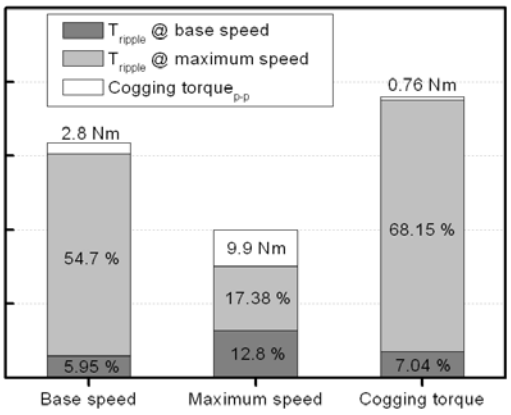

Fig. 7. Characteristics in optimal model of each response.

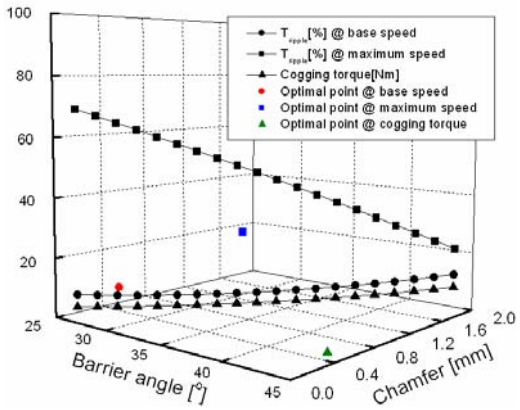

Fig. 8. Variation of each response according to design factors (SO: 8.68 mm).

V. Characteristic Analysis Including Losses And Discussion

When the optimization is performed in Section IV, the losses is not considered. Thus, if the losses is considered, the results of Table IX is not guaranteed because input current and β may be vary. In this Section, the characteristics of initial and optimal models are examined and analyzed when all the losses are considered.

A. Characteristic Prediction

The losses must be estimated to get the characteristic of each model. In this paper, R_c is calculated with the method proposed in Section III, and mechanical loss of all the models is the same and proportional to the square of mechanical speed [4]. At that time, the mechanical loss at 1000 rpm is standard, and it is defined as 0.5% of rated output power. Table X shows final results of each model considering the losses. The characteristic of the optimal model at the maximum speed is somewhat different as compared with other models. That is generated because of decrease of flux linkage by the chamfer. Therefore, as the optimization is performed at the maximum speed, the restrictions are required to satisfy the characteristics given in the specifications.

B. Torque Characteristic of Each Model

The torque waveform at the base and maximum speed and cogging torque of each model are shown in Fig. 9 and Fig. 10. At the base speed, the conditions, input current and β, of initial model are not greatly changed as compared with the original that because the influence of mechanical and iron loss is small. However, β of the optimized models considerably varies due to the decrease of back-EMF. So, torque ripple displayed in Fig. 9 differs from those given in Table IX.

VI. Conclusion

In this paper, an optimization method was proposed to improve torque performance of the IPMSM with concentrated winding and wide speed range, and the results by the method showed the optimization shape in each speed region is different. Moreover, as the optimal design is performed at the maximum speed, the particular care is required. Finally, the optimization direction of the IPMSM with concentrated winding operated in the wide speed range must be changed according to the application of the IPSMS.

References

[1] John M. Miller, *Propulsion systems for hybrid vehicles*, The Institution of Electrical Engineers, 2004.

[2] Mohammad S. Islam, S. Mir, T. Sebastian, and S. Underwood, "Design consideration of sinusoidally excited permanent magnet machines for low torque ripple applications," *in Conf. Rec. IEEE-IAS Annu. Meetings*, 2004, CD-ROM.

[3] M. Sanada, K. Hiramoto, S. Morimoto, and Y. Takeda, "Torque ripple improvement for synchronous reluctance motor using an asymmetric flux barrier arrangement," *IEEE Trans. Ind. Applicat.*, vol. 40, no. 4, pp. 1076-1082, July/August 2004.

[4] S. Morimoto, Y. Tong, Y. Takeda, and T. Hirasa, "Loss minimization control of permanent magnet synchronous motor drives," *IEEE Trans. Ind. Electron.*, vol. 41, no. 5, pp. 511-517, Oct. 1994.

[5] J. J. Lee, Y. K. Kim, H. Nam, K. H. Ha, J. P. Hong, and D. H. Hwang, "Loss distribution of three phase induction motor fed by pulsewidth-modulated inverter," *IEEE Trans. Magn.*, vol. 40, no. 2, pp. 762-765, Mar. 2004.

[6] S. Morimoto, Y. Takeda, and T. Hirasa, "Current phase control methods for permanent magnet synchronous motors," *IEEE Trans. Power Electron.*, vol. 5, no. 2, pp. 133-138, April 1990.

[7] S. Morimoto, and Y. Takeda, "Machine parameters and performance of interior permanent magnet synchronous motors with different permanent magnet volume," *Elec. Eng. in Japan*, vol. 131, no. 4, pp. 1403-1408, 2000.

[8] Douglas C. Montgomery, *Design and Analysis of Experiments*, John Wiley & Sons, 2001.

[9] Raymond H. Myers and Douglas C. Montgomery, *Response Surface Methodology: Process and Product Optimization Using Design Experiments*, John Wiley & Sons, 1995.

[10] J. T. Li, Z. J. Liu, M. A. Jabbar, and X. K. Gao, "Design optimization for cogging torque minimization using response surface methodology," *IEEE Trans. Magn.*, vol. 40, no. 2, pp. 1176-1179, March 2004.

TABLE IX
COMPARISON BETWEEN RESULTS BY EACH FITTED MODEL AND FEA

Optimal model @ base speed						Optimal model @ maximum speed						Optimal model @ cogging torque					
$\hat{Y}_{Tr}$ @base	*FEA*	$\hat{Y}_{Tr}$ @max.	*FEA*	$\hat{Y}_{CT}$	*FEA*	$\hat{Y}_{Tr}$ @base	*FEA*	$\hat{Y}_{Tr}$ @max.	*FEA*	$\hat{Y}_{CT}$	*FEA*	$\hat{Y}_{Tr}$ @base	*FEA*	$\hat{Y}_{Tr}$ @max.	*FEA*	$\hat{Y}_{CT}$	*FEA*
5.95	5.62	54.7	62.3	2.8	2.86	12.8	12.4	17.4	20.7	9.9	9.6	7.0	6.9	68.2	70.7	0.76	0.8

where input current and β at the base and maximum speed are the same those of the initial designed IPMSM mentioned in Section III.

TABLE X
FINAL RESULTS OF EACH MODEL CONSIDERING LOSSES

Model	Back-EMF [V_{rms}]	THD [%]	R_c [Ω]	@ Base speed							@ Maximum speed						
				I_a [A]	β [°]	W_c [kW]	W_i [W]	Eff. [%]	L_d [mH]	L_q [mH]	I_a [A]	β [°]	W_c [kW]	W_i [W]	Eff. [%]	L_d [mH]	L_q [mH]
Initial	101.3	13.4	306.4	65	39.3	1.83	95.1	90.9	3.11	4.94	67.4	80.8	1.97	64.2	86.3	3.58	4.72
Optimal @ base	99.7	2.8	308.7	65	34.1	1.83	91.9	90.9	3	4.62	67.2	82	1.96	53.2	86.4	3.41	5.35
Optimal @ max.	93	7.5	275	67.3	31.9	1.97	100	90.2	2.67	4.28	67.4	81.8	1.97	57.8	85.9	3.03	4.94
Optimal @ CogT	100.7	3.9	310.7	64.6	34	1.81	91.6	90.9	3.03	4.63	65	82.3	1.83	52.2	86.4	3.47	5.71

where Back-EMF is the value at the no-load and base speed, and THD is total harmonic distortion of Back-EMF.

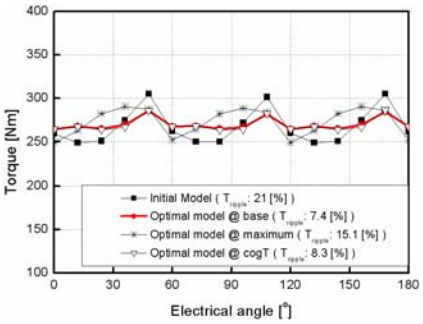

(a) @ Base speed

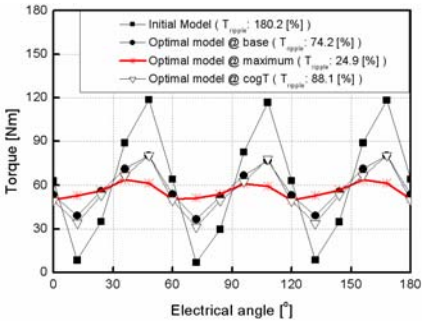

(b) @ Maximum speed

Fig. 9. Torque comparison of each model.

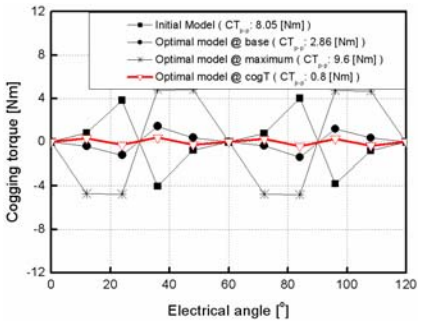

Fig. 10. Cogging torque comparison of each model

2007 Vehicle Power and Propulsion Conference

September 9 – 12, 2007

Wyndham (Sheraton Arlington) Hotel, DFW South Arlington, Texas, USA

- **Begin**
- **CD Help**
- **Preamble**
- **Technical Program**
- **Author Index**
- **Search**

IEEE Catalog Number: 07EX1461C

ISBN: 0-7803-9761-4

Co-Sponsored by:

Special Session 7: Electromechanical actuators for Vehicular Applications
Session Chair: Dr. Jin Hur
KETRI, South Korea
September 12, 2007
8:00 am – 9:00 am
Venue: SUPERBOWL – I

Characteristic Analysis and Comparison of IPMSM for HEV According to Pole and Slot Combination
Jae-Woo Jung, Jung-Pyo Hong and Young-Kyoun Kim[1]; *Hanyang Univ., [1]Korea Electronics Institute, S. Korea.*

Investigation on Characteristics and Optimal Shapes of Interior PM Synchronous Motor for Electric Vehicle Application
Sung-Il Kim, Jung-Pyo Hong and Jin Hur[1]; *Hanyang University, [1]Korea Electronics Technology Institute, S. Korea.*

Development of an Electric Driven Pump Unit for Electro-Hydraulic Power Steering of 42V Automobile
Se-hyun Rhyu, Yong-kyoun Kim, Jun-hyuk Choi, Jin Hur and Doo-hyung Lee[1]; *Korea Electronics Technology Institute, [1]Hyundai MOBIS, S. Korea.*

Post-break session: 10:30 am – 12:00 pm

Dynamic Control of Hybrid Energy Storage System for Mild HEV
Baek Haeng Lee, Dong Hyun Shin, Hyun Sik Song[1], Jin Beom Jeong[1], Hee Jun Kim and Byeong Woo Kim[2]; *Hanyang University, [1]Korea Automotive Technology Institute (KATECH), [2]Ulsan University, S. Korea*

The Development of Hybrid Electric Compressor Motor Drive System for HEV
Tae-Uk Jung, Sung-Ho Lee[1], Sung-Il Kim[2], Sung-Jun Park[3] and Jung-Pyo Hong[2]; *Kyungnam University, [1]Korea Institute of Industrial Technology, [2]Hanyang University, [3]Chonnam National University, S. Korea.*

Optimality and Reachability - Pseudo Boolean power Flows for multi-sourced Vehicle Topologies
George Kladis, John Economou, Antonios Tsourdos and Brian White*; Cranfield U.-Dept. of Aerospace Power and Sensors, USA.*